

Article

Applications of Nanofluids for the Thermal Enhancement in Radiative and Dissipative Flow over a Wedge

Naveed Ahmed ¹, Asifa Tassaddiq ², Rana Alabdan ², Adnan ³, Umar Khan ⁴, Saima Noor ⁵, Syed Tauseef Mohyud-Din ¹ and Ilyas Khan ^{6,7,*}

¹ Department of Mathematics, Faculty of Sciences, HITEC University Taxila Cantt, Taxila 47080, Pakistan; nidojan@gmail.com (N.A.); syedtauseefs@hotmail.com (S.T.M.-D.)

² College of Computer and Information Sciences, Majmaah University, Al Majmaah 11952, Saudi Arabia; a.tassaddiq@mu.edu.sa (A.T.); r.alabdan@mu.edu.sa (R.A.)

³ Department of Mathematics, Mohi-ud-Din Islamic University, Nerian Sharif, Azad Jammu and Kashmir 12080, Pakistan; adnanabbasi89@gmail.com

⁴ Department of Mathematics and Statistics, Hazara University, Mansehra 21310, Pakistan; umar_jadoon@hu.edu.pk

⁵ Department of Mathematics, COMSATS University Islamabad, Abbottabad 22010, Pakistan; saimanoor@ciit.net.pk

⁶ Faculty of Mathematics and Statistics, Ton Duc Thang University, Ho Chi Minh City 72915, Vietnam

⁷ Department of Mathematics, College of Science Al-Zulfi, Majmaah University, Al-Majmaah 11952, Saudi Arabia

* Correspondence: ilyaskhan@tdtu.edu.vn

Received: 19 December 2018; Accepted: 1 April 2019; Published: 14 May 2019



Abstract: The colloidal analysis for H₂O and EG (Ethylene Glycol) by considering the influence of radiative heat flux and viscous dissipation is not performed so far. This study is performed to fill up this gap. Therefore, the flow of water and ethylene glycol functionalized magnetite nanoparticles over a moving wedge is examined. For thermal enhancement, two different magnetite nanoparticles, namely CoFe₂O₄ (Cobalt ferrite) and Mn – ZnFe₂O₄ (Mn – Zn ferrite), diluted in the base fluids. Self-similar flow model of a nonlinear nature, containing the volume fraction of nanoparticles is obtained by using compatible similarity variables. For mathematical treatment of the model, the Runge-Kutta scheme is utilized, coupled with shooting techniques. The results for flow characteristics and significant physical parameters are graphically examined. A comprehensive comparative analysis has been made, which proved the reliability of the study.

Keywords: moving wedge; thermal radiation; magnetite nanoparticles; viscous dissipation; RK technique

1. Introduction

The colloidal study past a wedge geometry cannot be overlooked due to its extensive applications in many industrial, engineering zones. These comprised in thermal insulation, geothermal engineering, heat exchangers, and extraction of crude oil, etc. The flow regular liquids or nanofluids over a wedge geometry unlock a new window for researchers and scientists. Therefore, researchers and scientists focused in this direction and extended the model day by day with new advances.

The study of many fluids over a stationary or non-stationary wedge is of the important research area in the field of fluid dynamics. Firstly, Rajagopal et al. [1] reformed the work of Falkner Skan [2,3]. They investigated the flow behavior of second grade liquid over a stationary wedge. Afterwards, Hartree solved the Falkner Skan boundary layer flow model [4]. The behavior of the fluid temperature

over a static wedge was reported in [5]. Watanabe studied forced free convection by considering the influence of Lorentz force and suction or injection [6,7]. Koh et al. discussed the alterations due to various quantities on shear stresses and the local nusselt number [8]. Kumari et al. examined a theoretical investigation of the mixed convection wedge flow [9]. Further, Chamkha et al. [10] reported the flow over a thermally stratified wedge.

El-Dabe et al. reported the numerical treatment for casson fluid [11]. The effects of different parameters of self-similar nature was described in his study. Ishak et al. extended the model for micropolar fluid over a non-stationary wedge [12,13]. Rashidi et al. described the influence of Lorentz force on flow of viscoelastic fluid [14]. Su et al. discussed the mixed convective flow over a stretching wedge by considering the effects of magnetic field and thermal radiation [15]. In 2013, Mukhopadhyay et al. analyzed the flow of casson fluid by considering the geometry of the symmetric wedge [16]. They also described the effects of various emerging parameters for the heat transfer.

In 2014, Hussanan et al. investigated the Falkner Skan flow of unsteady nature over a wedge that was embedded in the porous medium [17]. Stimulus of the Joule heating and the concentration gradients in the flow regimes emerged in their study. In 2010, Kandasamy et al. reported the chemically reacting flow over a porous wedge [18]. The impact of the radiative heat flux and the suction or blowing was presented in the study. The influences of cross diffusion in chemically heating Falkner Skan flow was reported in [19]. Hussanan et al. studied the flow over an oscillating plate and analyzed the influence of newtonian heating and the convective flow conditions in the flow regimes [20]. Magneto hydrodynamics flow of nanofluids by considering the influence of Lorentz force, resistive heating, and velocity slip condition, as reported in [21]. The influence of suction or blowing in the flow characteristics past a wedge was investigated in [22]. Rahman et al. examined the hydromagnetic flow by considering the heat generation/absorption parameter [23]. In 2011, Yacob et al. extended the flow over a non-stationary wedge for nanofluids [24]. Khan et al. lately reported the bio-convection dissipative model over a wedge when considering the influences of porosity and gyrotactic microorganisms and nanoparticles [25]. The effects of the newtonian heating and other pertinent flow parameters on the flow characteristics are part of his analysis. In 2017, Khan et al. investigated the thermal enhancement in MHD flow past a wedge [26].

In 2016, Ullah et al. presented the non-Newtonian fluid model over a stretchable sheet [27]. They accounted the impacts of mixed convection and chemical reaction in the flow regimes. Thermal enhancement in the ferro fluid by considering the cylindrical shaped nanoparticles over a vertical channel investigated by Khalid et al. in [28]. The influences of the Ag nanoparticles on poiseuille flow by taking the influence of chemical reaction, thermal radiation, and cross diffusion was presented by Aman et al. [29]. The second grade fluid model and the nanofluid flow in an oblique channel and Riga plates were reported in [30,31], respectively. Ahmed et al. examined the stimulus of an effective Prandtl model for the flow characteristics [32]. The influence of thermal radiation on viscous incompressible between oblique walls was examined by Adnan et al. [33]. For further useful study regarding Newtonian, non-Newtonian, and nanofluids while considering the various flow conditions in different geometries are presented in [34–46].

From keen literature review, it is noticed that the colloidal analysis of CoFe_2O_4 (Cobalt ferrite) and $\text{Mn} - \text{ZnFe}_2\text{O}_4$, by considering water and ethylene glycol as carrier liquids in the existence of radiative heat flux and viscous dissipation, is not presented so far. This study is presented to fill up this significant gap. The influences of the parameters are graphically explored for flow characteristics and heat transfer rate with comprehensive discussion, and fascinating results for heat transfer rate were found for both type of nanofluids.

2. Model Formulation

The radiative and dissipative colloidal suspension of water and ethylene glycol suspended by cobalt ferrite and Mn-Zn ferrite is under consideration over a non-static wedge. The flow obeys the characteristics of incompressible flow. The flow configuration is taken in the Cartesian coordinate

system. $U_w = U_\infty x^m$ and $u_w = U_w x^m$ denote the main stream and wedge velocities, respectively. Furthermore, $\lambda = 2m(m + 1)^{-1}$ represents the Hartree pressure corresponding to $\lambda = (\pi)^{-1}\Omega$. Moreover, the temperature of the wedge wall is a function of x and is $T_w(x) = T_\infty + \frac{A}{x^{2m}}$, where T_∞ shows the free stream temperature. Figure 1 depicts the flow configuration with coordinate axes:

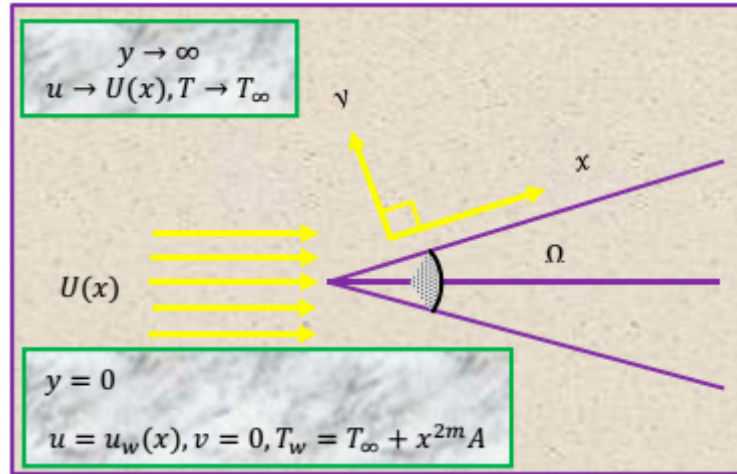


Figure 1. Flow Configuration and Coordinates.

In the light of aforesaid assumptions, the following set of PDE's govern the flow of H_2O and $C_2H_6O_2$ suspended by cobalt ferrite and Mn-Zn ferrite nanoparticles [47,48]:

$$\frac{\partial u}{\partial x} + \frac{\partial v}{\partial y} = 0, \tag{1}$$

$$u \frac{\partial u}{\partial x} + v \frac{\partial u}{\partial y} = U(x) \frac{dU(x)}{dx} + \frac{\mu_{nf}}{\rho_{nf}} \left(\frac{\partial^2 u}{\partial y^2} \right), \tag{2}$$

$$u \frac{\partial T}{\partial x} + v \frac{\partial T}{\partial y} = \frac{k_{nf}}{(\rho c_p)_{nf}} \left(\frac{\partial^2 T}{\partial y^2} \right) + \frac{1}{(\rho c_p)_{nf}} \left(\frac{\partial u}{\partial y} \right)^2 - \frac{16\sigma^* T_\infty^3}{3k(\rho C_p)_{nf}} \left(\frac{\partial^2 T}{\partial y^2} \right). \tag{3}$$

Here, Equation (1) shows the conservation law for mass and Equation (2) represents the momentum equation. Furthermore, velocity components in horizontal and vertical directions are denoted by u and v , respectively. Additionally, $U(x)$ shows main stream velocity, Temperature T , heat capacity $(\rho C_p)_{nf}$ dynamic viscosity μ_{nf} , effective thermal conductivity k_{nf} , and mean adsorption coefficient is k :

For our flow model, the following are the feasible boundary conditions [48]:

$$u_{y=0} = u_w(x), v_{y=0} = 0, T_{y=0} = T_\infty + \frac{A}{x^{2m}}, \tag{4}$$

$$u_{y \rightarrow \infty} \rightarrow U(x), T_{y \rightarrow \infty} \rightarrow T_\infty. \tag{5}$$

The set of self-similar transformations are as under [49]:

$$u = \frac{\partial \psi}{\partial y}, v = -\frac{\partial \psi}{\partial x}, \psi = \sqrt{\frac{2\nu_f x U(x)}{(m+1)}} F(\eta), \eta = \sqrt{\frac{(m+1)U(x)}{2\nu_f x}} y, \beta(\eta) = \frac{T - T_\infty}{T_w - T_\infty}. \tag{6}$$

The following nanofluid characteristics are utilized [50]:

$$\rho_{nf} = (1 - \phi)\rho_f + \phi\rho_s, \tag{7}$$

$$(\rho C_p)_{nf} = (1 - \phi)(\rho C_p)_f + \phi(\rho C_p)_s \tag{8}$$

$$k_{nf} = k_s \left[\frac{(k_s + 2k_f) - 2\phi(k_f - k_s)}{(k_s + 2k_f) + \phi(k_f - k_s)} \right] \tag{9}$$

In Equations (7)–(9), ϕ is volume fraction, $(\rho C_p)_f$ is heat capacity of carrier fluids, k_s shows nanoparticles thermal conductivity, k_f is base liquid thermal conductivity, and ρ_s and ρ_f are the dynamic viscosities of nanoparticles and base liquid, respectively.

Table 1 describes the thermal and physical characteristics for base liquids and nanoparticles.

Table 1. Thermal and Physical characteristics [49,50].

Properties	ρ (kg/m ³)	c_p (J/Kg K)	k (W/mk)	Pr
H ₂ O	997.1	4179	0.613	6.96
C ₂ H ₆ O ₂	1116.6	2382	0.249	204
CoFe ₂ O ₄	4907	700	3.7
Mn – ZnFe ₂ O ₄	4900	800	5.0

By entreating the self-similar transformations that are given in Equation (6), the following non-dimensional model is attained:

$$F''' + \left[1 - \phi + \frac{\phi \rho_s}{\rho_f} \right] (1 - \phi)^{2.5} (FF'' + \lambda(1 - F'^2)) = 0, \tag{10}$$

$$\left[1 + Rd \left\{ \frac{((k_s + 2k_f) - 2\phi(k_f - k_s))}{((k_s + 2k_f) + \phi(k_f - k_s))} \right\}^{-1} \right] \beta'' + \left[\frac{((k_s + 2k_f) - 2\phi(k_f - k_s))}{((k_s + 2k_f) + \phi(k_f - k_s))} \right]^{-1} \left[\frac{PrF\beta' - 2\lambda PrF'\beta}{\left\{ (1 - \phi) + \frac{\phi(\rho C_p)_s}{(\rho C_p)_f} \right\}^{-1}} + PrEcF'^2 \right] = 0. \tag{11}$$

Particular conditions at wedge surface and far from the wedge surface are as under:

At $\eta = 0$:

$$F(\eta) = 0, F'(\eta) = \gamma, \beta(\eta) = 1, \tag{12}$$

At $\eta \rightarrow \infty$:

$$F'(\eta) \rightarrow 1, \beta(\eta) \rightarrow 0. \tag{13}$$

Further, self-similar parameters emerged in the model are:

$$Pr = \frac{\mu_f(c_p)_f}{k_f}, Rd = \frac{16\sigma^* T_\infty^3}{3k_f k}, Ec = \frac{U^2(x)}{(c_p)_f (T_w - T_\infty)}, \text{ and } \gamma = \frac{U_w}{U_\infty}.$$

The dimensional form for shear stresses and local nusselt number are:

$$C_F = \frac{\mu_{nf}}{\rho_f U^2(x)} \left(\frac{\partial u}{\partial y} \right) \downarrow_{y=0} \tag{14}$$

$$Nu_x = \left[\frac{-xk_{nf}}{k_f(T_w - T_\infty)} \right] \left(\frac{\partial T}{\partial y} \right) \downarrow_{y=0}, \tag{15}$$

After simplifications, Equations (14) and (15) reduced into the following formula:

$$C_F \sqrt{Re_x} = (1 - \phi)^{-2.5} F''(0),$$

$$Nu_x (Re_x)^{-\frac{1}{2}} = - \left[\frac{((k_s + 2k_f) - 2\phi(k_f - k_s))}{((k_s + 2k_f) + \phi(k_f - k_s))} \right] \beta'(0),$$

here, $Re_x = \frac{xU(x)}{\nu_f}$ is indicates the local Reynold number.

3. Mathematical Analysis

The model under consideration is nonlinear in nature. For such a type of models, exact solutions are very rare and very difficult to calculate. In such a situation, numerical computation is reliable. Thus, the Runge–Kutta scheme [51] is adopted for particular flow model. In order to apply the aforesaid scheme, firstly the flow model is reduced into a coupled first order Initial Value Problem (IVP). For the said purpose, the following key transformations are used:

$$y_1 = F, y_2 = F', y_3 = F'', y_4 = \beta, y_5 = \beta'. \tag{16}$$

To initiate the scheme, firstly transform the model in the following manner:

$$F''' = - \frac{[1 - \phi + \frac{\phi \rho_s}{\rho_f}]}{(1 - \phi)^{-2.5}} (FF'' + \lambda(1 - F'^2)), \tag{17}$$

$$\beta'' = - \left[1 + \frac{Rd}{A_3} \right] \left[A_3 \right]^{-1} \left\{ (1 - \phi) + \frac{\phi(\rho_{cp})_s}{(\rho_{cp})_f} \right\} (PrF\beta' - 2\lambda PrF'\beta) + PrEcF''^2. \tag{18}$$

Here, $A_3 = \left\{ \frac{((k_s + 2k_f) - 2\phi(k_f - k_s))}{((k_s + 2k_f) + \phi(k_f - k_s))} \right\}$.

After the utilization of transformations that are defined in Equation (16), the attained system is:

$$\begin{bmatrix} y_1' \\ y_2' \\ y_3' \\ y_4' \\ y_5' \end{bmatrix} = \begin{bmatrix} y_2 \\ y_3 \\ - \frac{(y_1 y_3 + \lambda(1 - (y_2)^2))}{[1 - \phi + \frac{\phi \rho_s}{\rho_f}]^{-1} (1 - \phi)^{-2.5}} \\ y_5 \\ - \left[1 + \frac{Rd}{A_3} \right] \left[A_3 \right]^{-1} \left[\frac{Pr y_1 y_5 - 2\lambda Pr y_2 y_4}{\left\{ (1 - \phi) + \frac{\phi(\rho_{cp})_s}{(\rho_{cp})_f} \right\}^{-1}} + PrEc(y_3)^2 \right] \end{bmatrix} \tag{19}$$

The corresponding initial conditions are in the following way.

$$\begin{bmatrix} y_1 \\ y_2 \\ y_3 \\ y_4 \\ y_5 \end{bmatrix} = \begin{bmatrix} 0 \\ \gamma \\ n_1 \\ 1 \\ n_2 \end{bmatrix}. \tag{20}$$

Now, Mathematica 10.0 is applied for the computation purpose.

4. Graphical Results and Discussion

The ingrained physical quantities in the flow model, like ϕ , Pr , Ec , and Rd significantly affect the flow characteristics, shear stresses, and local rate of heat transfer. This section described the impacts of

above-mentioned physical parameters in the flow characteristics. Three different cases of the nanofluids flow is discussed:

- i. When the wedge and colloidal suspension move in the opposite direction. The parameter $\gamma < 0$ elucidates such flow.
- ii. When the wedge and colloidal suspension move in the same sense. This type of flow occurs for $\gamma > 0$.
- iii. The static wedge case is considered for $\gamma = 0$.

Further, the numerical values obtained for shear stress and compared with literature which confirms the reliability of the study.

The influences of pressure gradient parameter called Hartree pressure plays a vibrant role on the velocity distribution of the nanofluids. Figure 2 shows these effects for assisting, opposing, and static wedge condition. It is examined that, by increasing the pressure, the nanofluids particles move promptly in the region $0 \leq \eta \leq 3$. Near the surface of the wedge, the particles momentum drops due to the friction factor between the surface and the nanofluids particles. The friction between the rest of the layer's declines, which allows the particles move freely. Therefore, the momentum of the particles increases. For the static wedge condition, the velocity slowly arises in comparison with assisting and opposing flow conditions. The opposing motion of the wedge reduces the nanofluids velocity and the movement of the wedge in the direction of the flow increases the velocity field $F'(\eta)$. The changes in the velocity are almost similar for both kinds of the nanofluids.

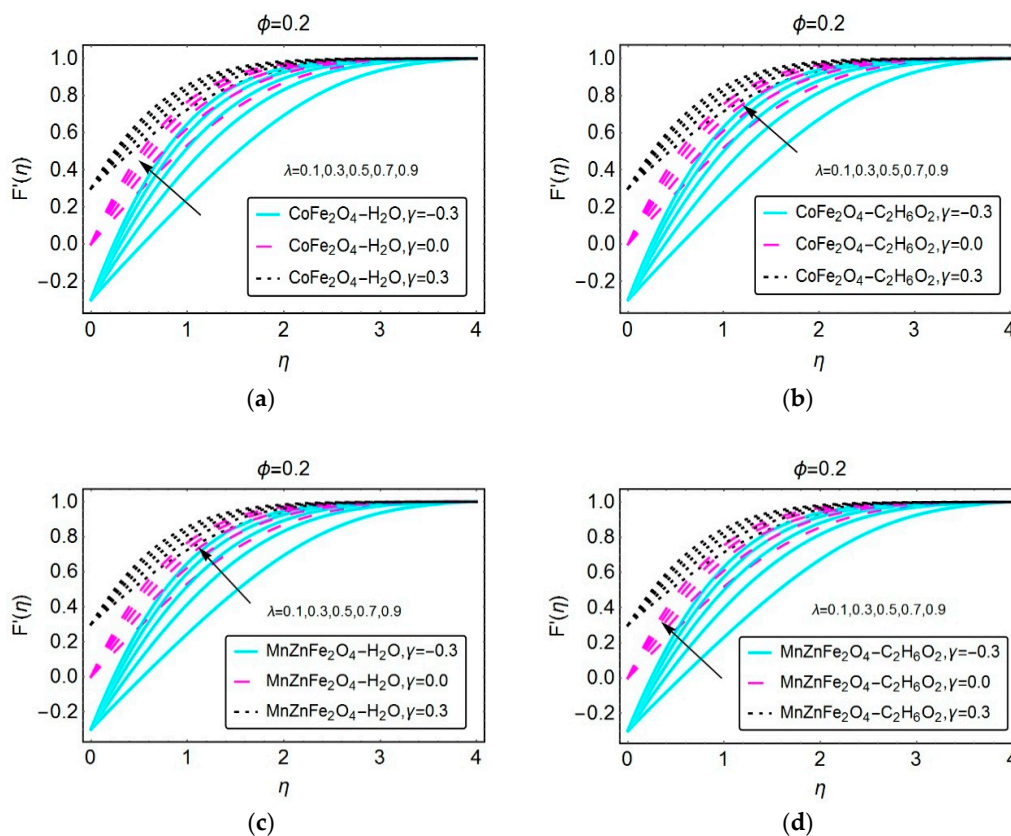


Figure 2. Alterations in the velocity distribution for (a) $\text{CoFe}_2\text{O}_4 - \text{H}_2\text{O}$; (b) $\text{CoFe}_2\text{O}_4 - \text{C}_2\text{H}_6\text{O}_2$; (c) $\text{MnZnFe}_2\text{O}_4 - \text{H}_2\text{O}$; (d) $\text{MnZnFe}_2\text{O}_4 - \text{C}_2\text{H}_6\text{O}_2$ nanofluids by varying λ .

Varying the flow parameters significantly alters the temperature distribution. These parameters are the radiation parameter, Eckert number fraction factor of the nanoparticles, and λ . These effects that are portrayed in Figures 3–6 for the nanofluids under consideration. It is examined that the

temperature enhances for the flow of water composed by the cobalt and Mn-Zn and drops for ethylene glycol based hosting fluid. These temperature effects are due to varying Hartree pressure and are displayed in Figure 3. For the opposing wedge condition, the nanofluids velocity drops, which is due to the particles slowly becoming colloid and alternately the temperature drops. On the other hand, for the assisting case, the collision between the particles increases due to the alike motion of the nanofluids and the wedge, which promptly enhances the temperature. These effects of the temperature $\beta(\eta)$, as highlighted in Figure 3 for feasible Hartree pressure gradient parameter λ .

It is prominent fact that the radiation parameter significantly enhances the temperature and hence it cannot be ignored. Figure 4 portrays the alterations in the temperature distribution $\beta(\eta)$ for increasing the radiation parameter. It is obvious that, for stronger thermal radiation, the temperature field significantly enhances. When the nanofluids and the wedge move in alike direction, then temperature the distribution becomes rapid in comparison with the static and opposing flow conditions, respectively. The dominating behavior of $\beta(\eta)$ is noted for ethylene glycol based nanofluids and for water based nanofluid; these variations are quite slow.

The impacts of the Eckert parameter on the temperature behavior $\beta(\eta)$ for both types of nanofluids that are elucidated in Figure 5. The temperature $\beta(\eta)$ arises for opposing condition and then asymptotically vanishes far from the surface. For alike movement of the nanofluids and the wedge, the behavior of the temperature is almost inconsequential.

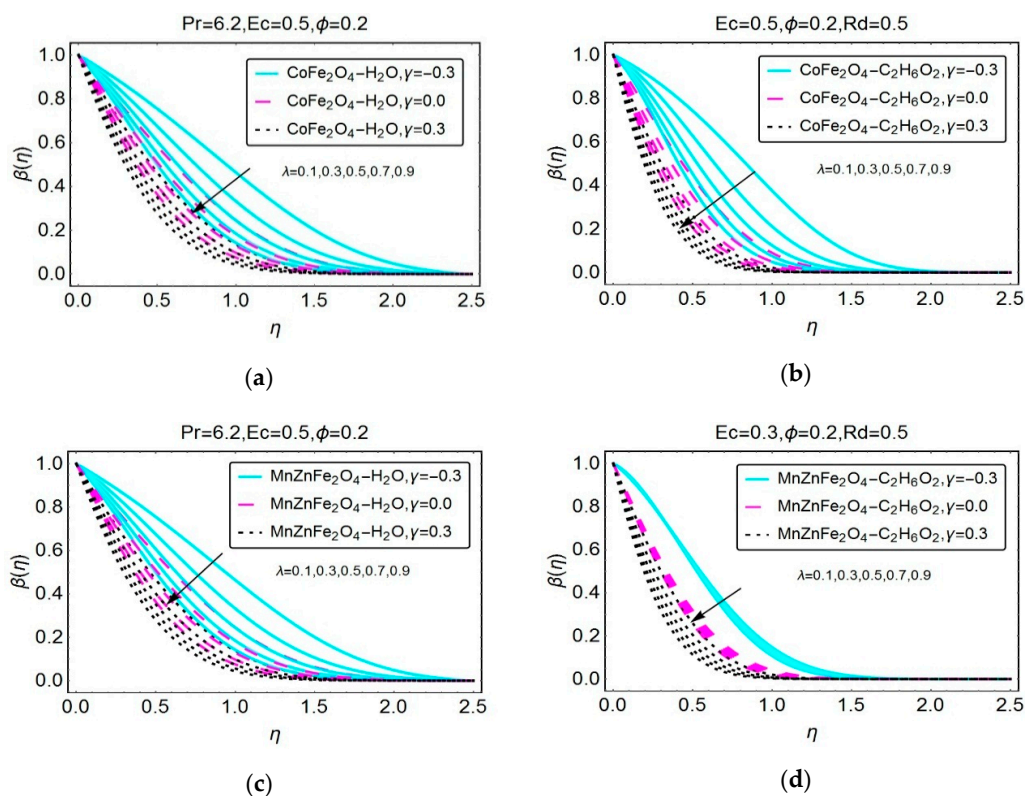


Figure 3. Alterations in the temperature distributions for (a) $\text{CoFe}_2\text{O}_4 - \text{H}_2\text{O}$; (b) $\text{CoFe}_2\text{O}_4 - \text{C}_2\text{H}_6\text{O}_2$; (c) $\text{MnZnFe}_2\text{O}_4 - \text{H}_2\text{O}$; (d) $\text{MnZnFe}_2\text{O}_4 - \text{C}_2\text{H}_6\text{O}_2$ nanofluids by varying λ .

It is a prominent fact that the thermal conductivity of the host liquids (water and ethylene glycol) is not up to the mark. However, mixing the cobalt and ferrite nanoparticles can enhance the thermal conductance of these liquids. The resultant composition then has better thermal enhancement characteristics. For this, the volume fraction factor ϕ plays the role of key ingredient. These effects are elaborated in Figure 6 for both nature of the nanofluids. It can be seen that, for static wedge flow, the temperature alterations are more obvious in comparison with the opposing flow. The temperature of the nanofluids shows asymptotic pattern far from the wedge.

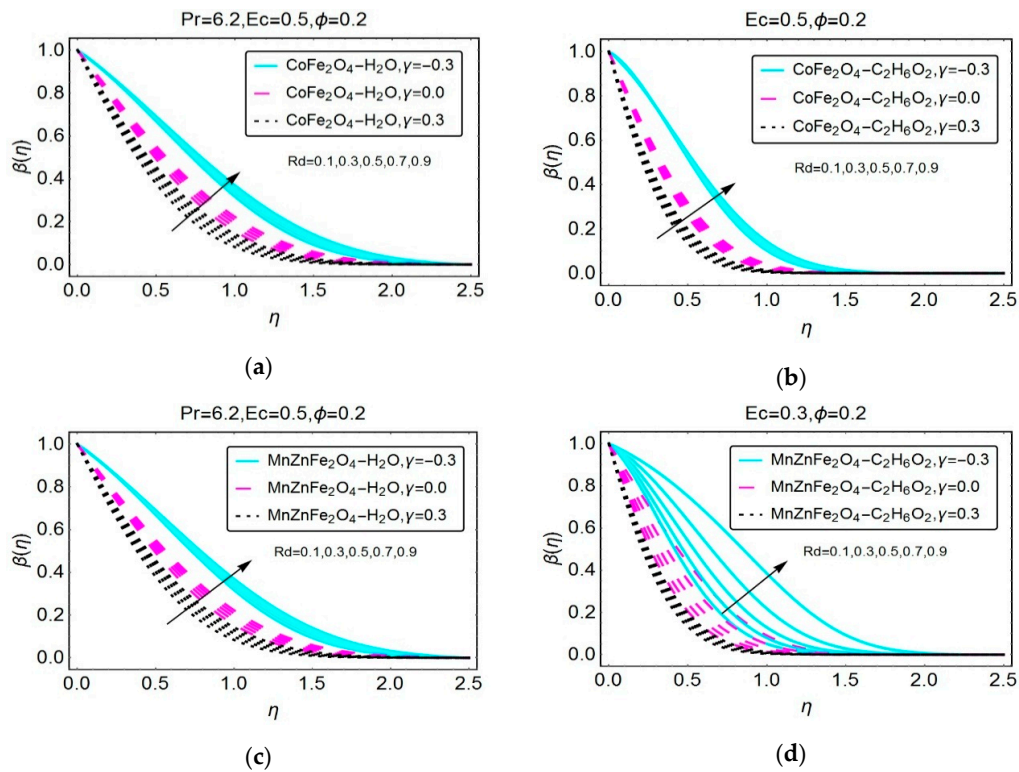


Figure 4. Alterations in the temperature distribution for (a) $\text{CoFe}_2\text{O}_4 - \text{H}_2\text{O}$; (b) $\text{CoFe}_2\text{O}_4 - \text{C}_2\text{H}_6\text{O}_2$; (c) $\text{MnZnFe}_2\text{O}_4 - \text{H}_2\text{O}$; (d) $\text{MnZnFe}_2\text{O}_4 - \text{C}_2\text{H}_6\text{O}_2$ nanofluids by varying Rd .

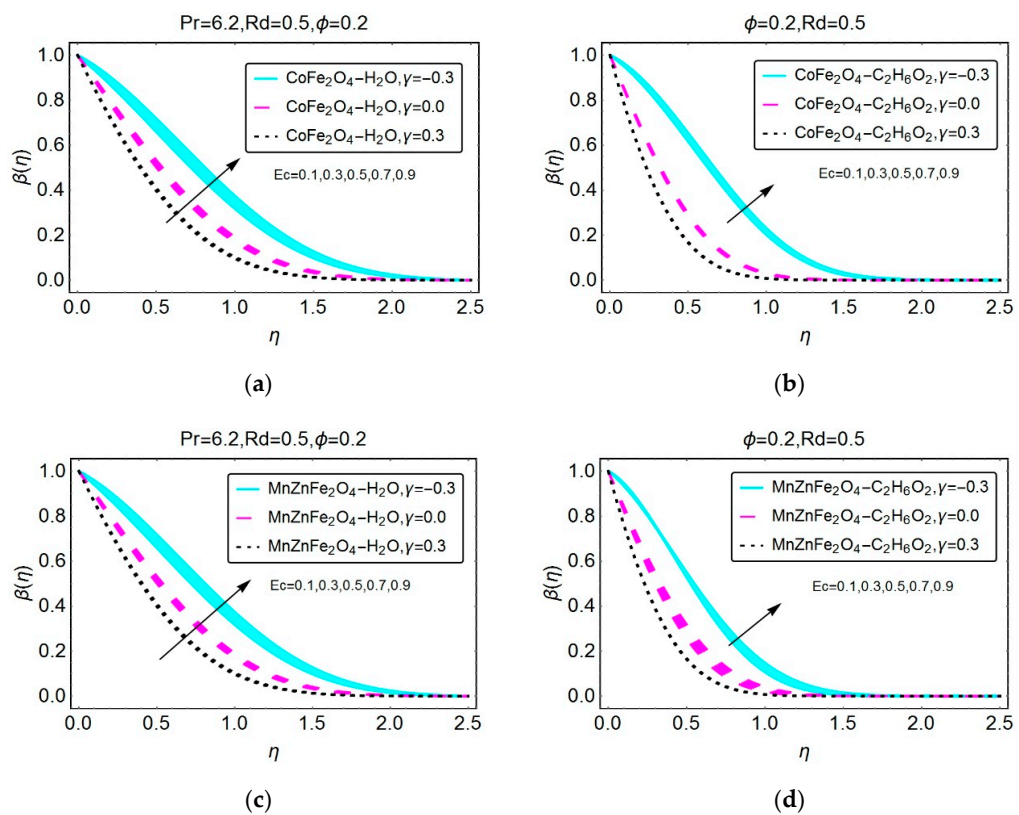


Figure 5. Alterations in the temperature distribution for (a) $\text{CoFe}_2\text{O}_4 - \text{H}_2\text{O}$; (b) $\text{CoFe}_2\text{O}_4 - \text{C}_2\text{H}_6\text{O}_2$; (c) $\text{MnZnFe}_2\text{O}_4 - \text{H}_2\text{O}$; (d) $\text{MnZnFe}_2\text{O}_4 - \text{C}_2\text{H}_6\text{O}_2$ nanofluids by varying Ec .

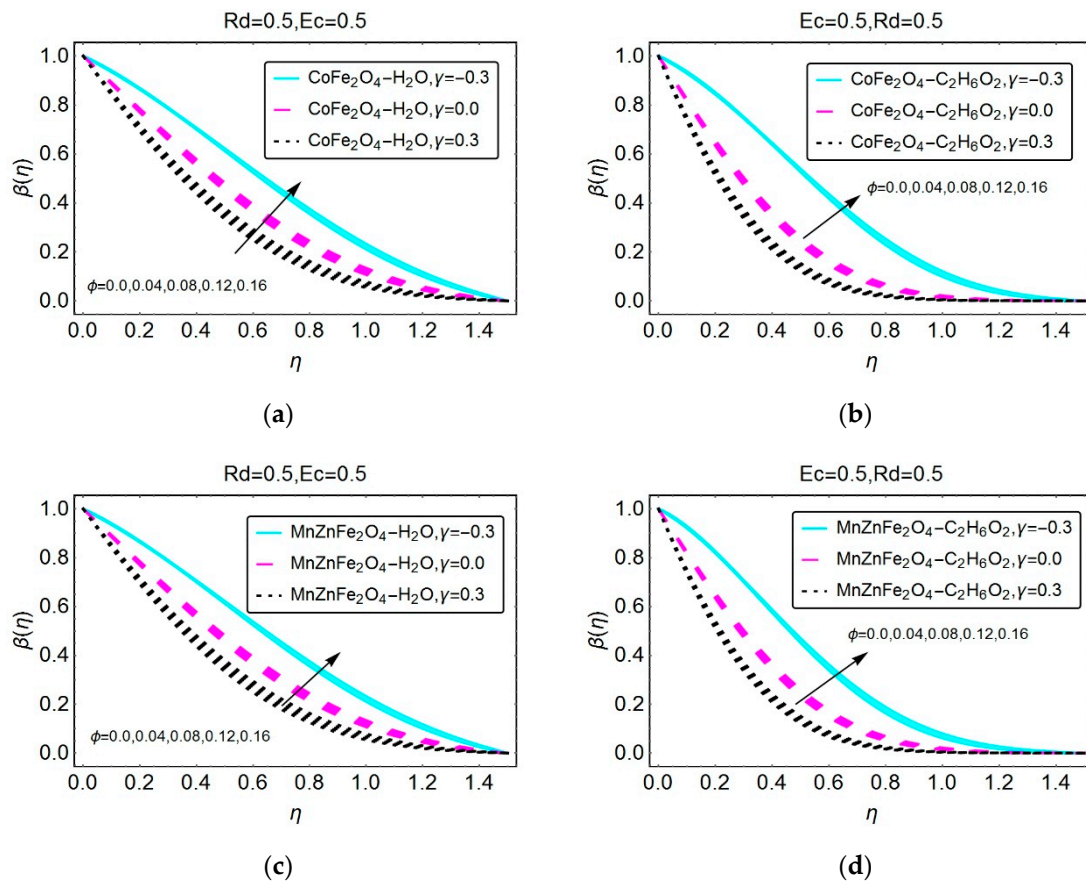


Figure 6. Alterations in the temperature distribution for (a) $\text{CoFe}_2\text{O}_4 - \text{H}_2\text{O}$; (b) $\text{CoFe}_2\text{O}_4 - \text{C}_2\text{H}_6\text{O}_2$; (c) $\text{MnZnFe}_2\text{O}_4 - \text{H}_2\text{O}$; (d) $\text{MnZnFe}_2\text{O}_4 - \text{C}_2\text{H}_6\text{O}_2$ nanofluids by varying ϕ .

The significance of the nondimensional physical quantities in the shear stresses and the heat transfer rate cannot be ignored. Since water and ethylene glycol taken as a regular liquids. For these liquids, the Prandtl number has a fixed value and is described in [52], respectively. Figures 7–11 elaborated the impacts of aforementioned parameters on the local heat transfer.

The variations in the local heat transfer rate by altering the radiation and volume fraction parameter described in Figure 7. The transfer rate is rapid for strong thermal radiation parameter R_d . For Ethylene glycol based nanofluids, drops in the local heat transfer rate are noted. For opposing flow, less amount of heat transfers at the wedge surface in comparison with the static and moving wedge, respectively. For smaller ϕ , the heat transfer rate is quite slow. Figure 8 highlights the impacts of fraction factor ϕ on the heat transfer at the wedge. The higher values of ϕ lead to increasing the behavior of the heat transfer. The up turns in the nusselt number are inspected for alike nanofluids flow. For the static wedge condition, the heat transfer slowly varies in comparison with opposing and assisting flow situations. The heat transfer quite rapidly arises for EG based nanofluid and effects of R_d and Hartree pressure elaborated in Figure 9.

The impacts of Hartree pressure versus Eckert number on the heat transfer rate are organized in Figure 10. The heat transfer reduces for Hartree pressure versus Eckert number E_c . By increasing the Eckert parameter, the heat transfers at the wedge surface arises drops. For EG based nanofluids, heat transfer promptly declines. Figure 11 elaborated on the influences of Hartree pressure versus volume fraction factor ϕ . The heat transfer enhances by altering the Hartree pressure and the volume fraction ϕ of the nanoparticles. For the opposing flow situation, heat transfers rapidly at the wedge surface. Further, it is examined that, for smaller λ and ϕ , the heat transfer slowly intensifies.

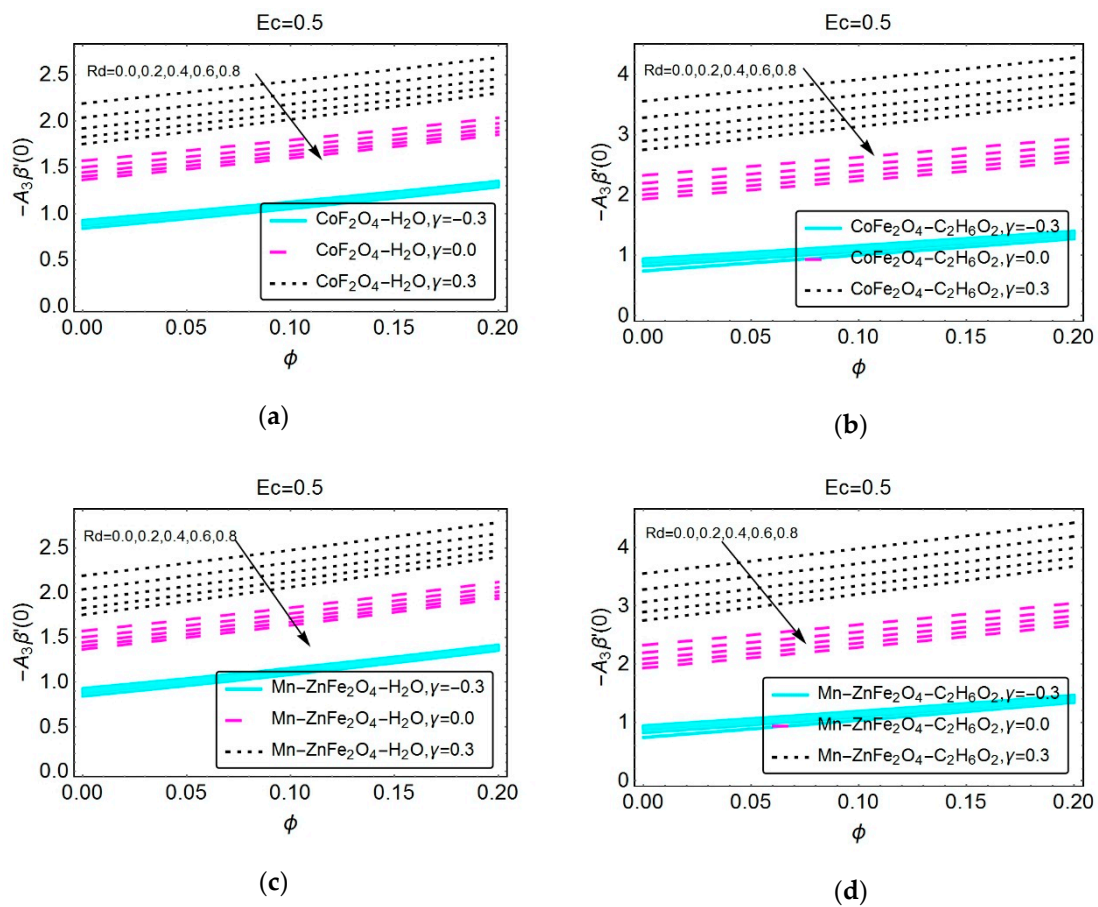


Figure 7. Alterations in the local nusselt number for (a) $\text{CoFe}_2\text{O}_4 - \text{H}_2\text{O}$; (b) $\text{CoFe}_2\text{O}_4 - \text{C}_2\text{H}_6\text{O}_2$; (c) $\text{MnZnFe}_2\text{O}_4 - \text{H}_2\text{O}$; (d) $\text{MnZnFe}_2\text{O}_4 - \text{C}_2\text{H}_6\text{O}_2$ nanofluids by varying Rd and ϕ .

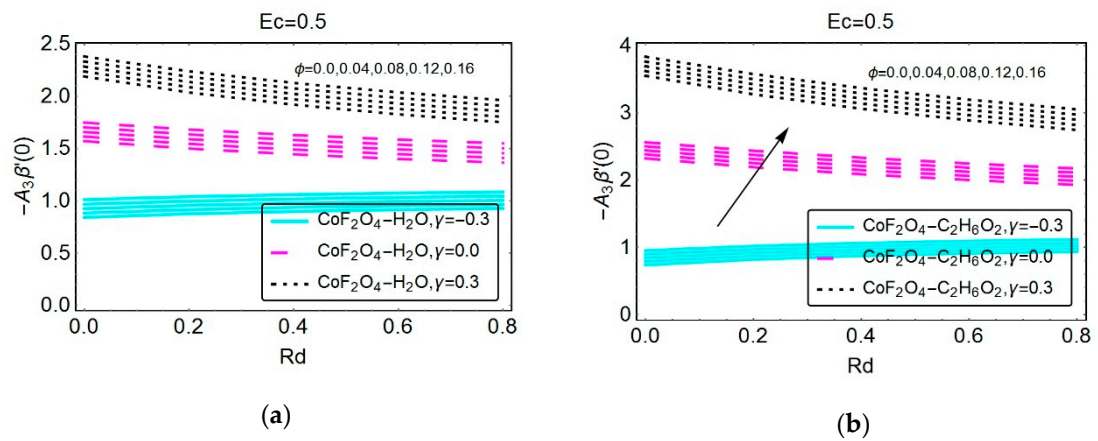


Figure 8. Cont.

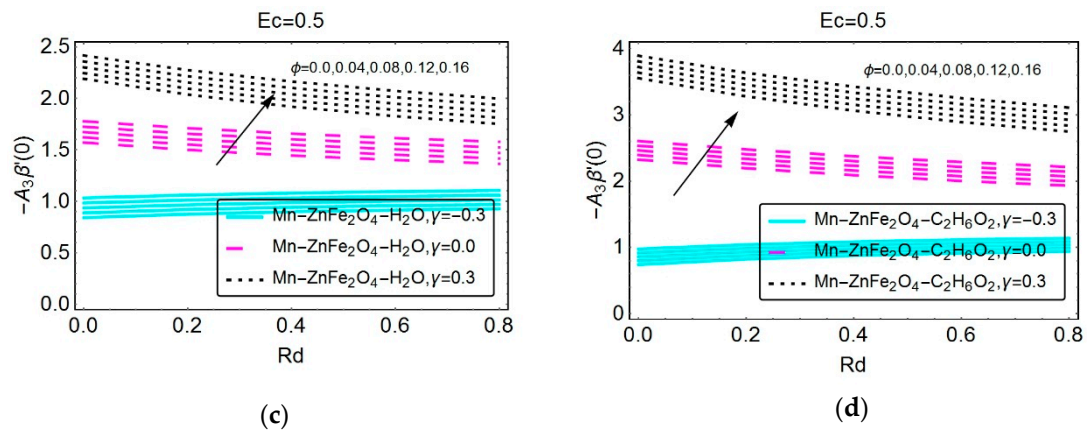


Figure 8. Alterations in the local nusselt number for (a) $\text{CoFe}_2\text{O}_4 - \text{H}_2\text{O}$; (b) $\text{CoFe}_2\text{O}_4 - \text{C}_2\text{H}_6\text{O}_2$; (c) $\text{MnZnFe}_2\text{O}_4 - \text{H}_2\text{O}$; (d) $\text{MnZnFe}_2\text{O}_4 - \text{C}_2\text{H}_6\text{O}_2$ nanofluids by varying ϕ .

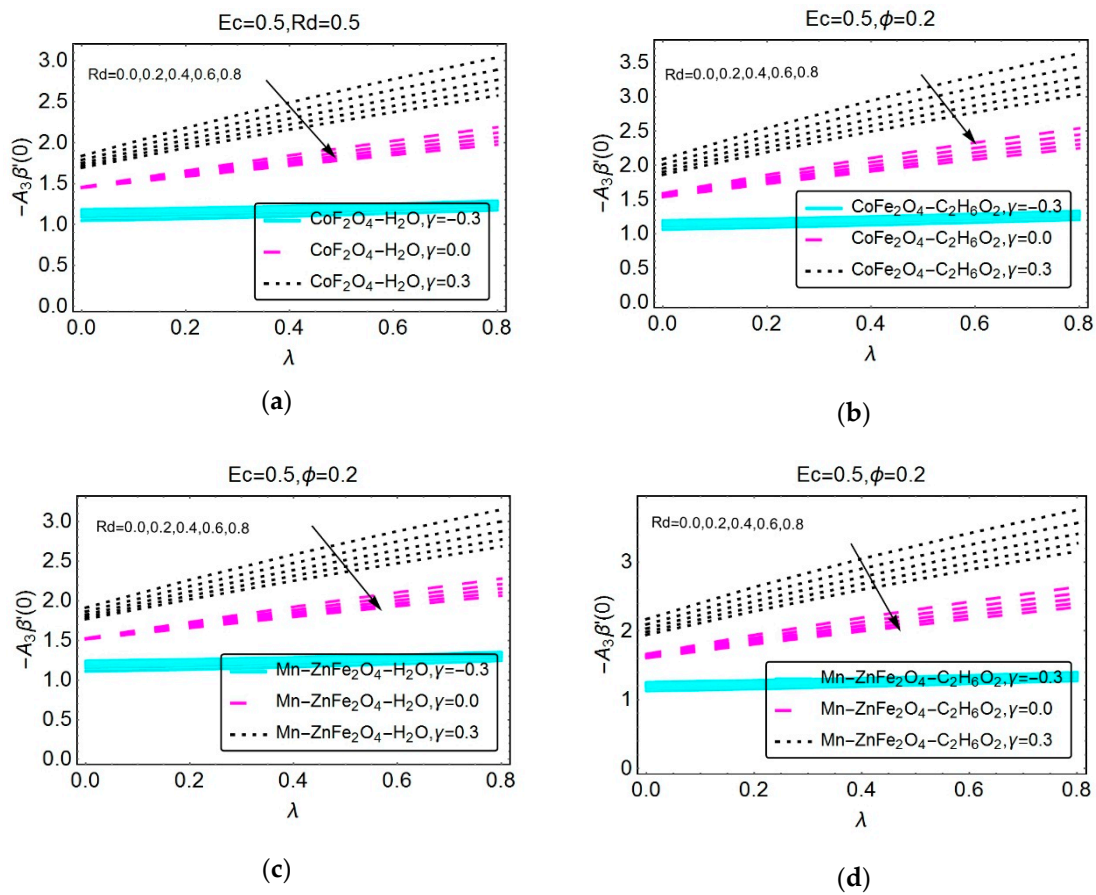


Figure 9. Alterations in the local nusselt number for (a) $\text{CoFe}_2\text{O}_4 - \text{H}_2\text{O}$; (b) $\text{CoFe}_2\text{O}_4 - \text{C}_2\text{H}_6\text{O}_2$; (c) $\text{MnZnFe}_2\text{O}_4 - \text{H}_2\text{O}$; (d) $\text{MnZnFe}_2\text{O}_4 - \text{C}_2\text{H}_6\text{O}_2$ nanofluids by varying Rd and λ .

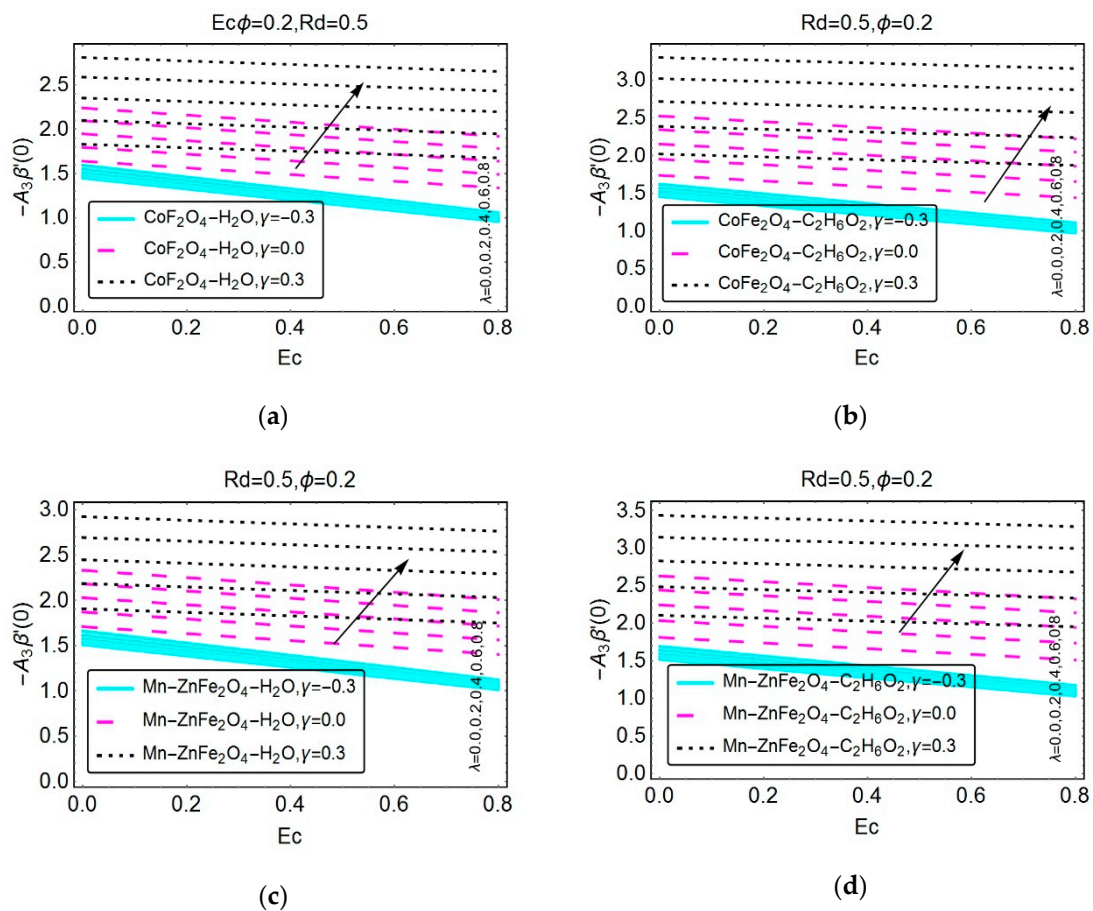


Figure 10. Alterations in the local nusselt number for (a) $CoFe_2O_4 - H_2O$; (b) $CoFe_2O_4 - C_2H_6O_2$; (c) $MnZnFe_2O_4 - H_2O$; (d) $MnZnFe_2O_4 - C_2H_6O_2$ nanofluids by varying λ and Ec .

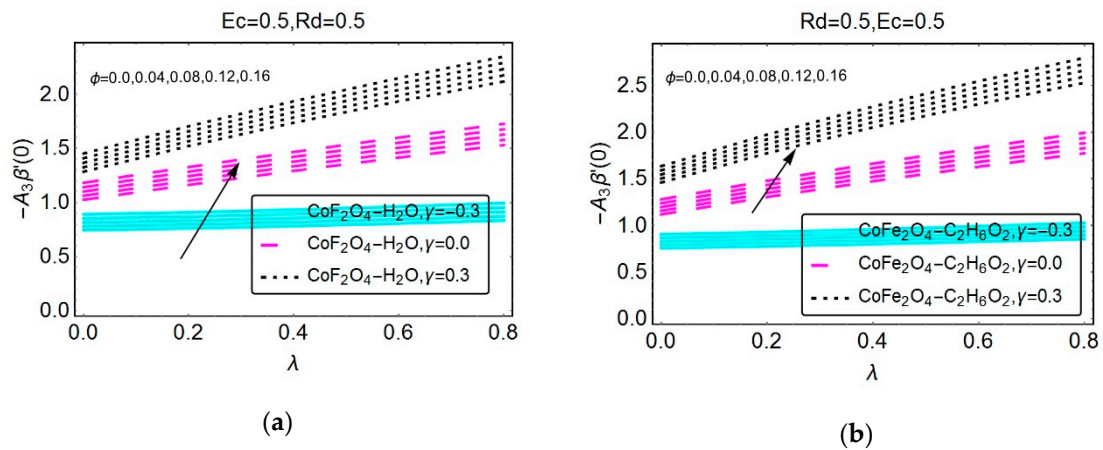


Figure 11. Cont.

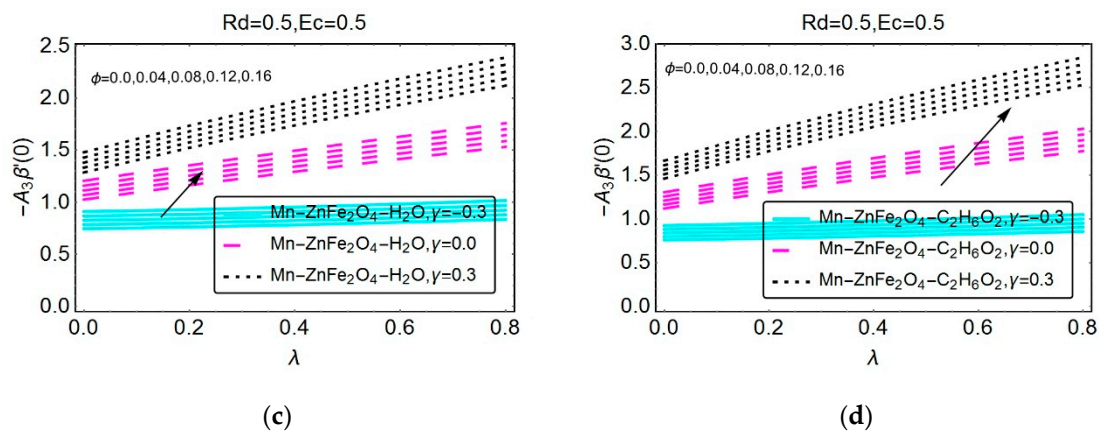


Figure 11. Alterations in the local nusselt number for (a) $\text{CoFe}_2\text{O}_4 - \text{H}_2\text{O}$; (b) $\text{CoFe}_2\text{O}_4 - \text{C}_2\text{H}_6\text{O}_2$; (c) $\text{MnZnFe}_2\text{O}_4 - \text{H}_2\text{O}$; (d) $\text{MnZnFe}_2\text{O}_4 - \text{C}_2\text{H}_6\text{O}_2$ nanofluids by varying ϕ and λ .

Table 2 presents the comparative analysis for shear stresses with existing results. It can be seen that, under certain restrictions on flow parameters, the presented results provoked the reliability of the study.

Table 2. Comparative analysis for $F''(0)$.

$\phi = \text{Rd} = \text{Ec} = \gamma = 0, \text{Pr} = 0.73, \lambda = \frac{2m}{m+1}$							
m	Present	[26]	[6]	[9]	[52]	[12]	[46]
0.0000	0.46959999	0.4695999	0.46960	0.46975	0.46972	0.4696	0.4696
0.0141	0.50461433	0.5046143	--	0.50472	0.50481	0.5046	0.5046
0.0435	0.56897778	0.5689777	0.56898	0.56904	0.56890	0.5690	0.5690
0.0909	0.65497886	0.6549788	0.65498	0.65501	0.65493	0.6550	0.6550
0.1429	0.73199857	0.7319985	0.73200	0.73202	0.73196	0.7320	0.7320
0.2000	0.80212563	0.8021256	0.80213	0.80214	0.80215	0.8021	0.8021
0.3333	0.92765362	0.9276536	0.92765	0.92766	0.92767	0.9277	0.9277
0.5000	1.03890351	1.0389035	1.03890	--	1.03890	--	--

5. Conclusions

The flow water and EG composed by CoFe_2O_4 and $\text{Mn} - \text{ZnFe}_2\text{O}_4$ nanoparticles are discussed over a wedge geometry. The resultant nanofluids model is numerically handled and the impacts of emerging flow quantities on the flow regimes and local heat transfer rate were comprehensively examined. It is examined that the Hartree pressure parameter enhances the velocity. The flow of nanofluids is rapid for assisting case in comparison with the static and opposing wedge conditions. The temperature of the nanofluids drops by altering the Hartree pressure. For assisting flow condition, the temperature $\beta(\eta)$ promptly drops. The radiation parameter enhances the nanofluids temperature. The heat transfer rate enhances for the volume fraction factor. Finally, the comparative analysis proved the validity of the study.

6. Future Directions

In future, the work can be extended for the colloidal analysis by considering the impacts of other physical phenomenon like Lorentz forces, resistive heating, heat generation/absorption etc. Further, the comparative analysis can be explored for various nanofluids theoretical models which will be an interesting and fruitful analysis from industrial point of view.

Author Contributions: Conceptualization, U.K., I.K. and Adnan; methodology, Adnan, N.A.; software, S.N.; validation, A.T. and R.A., writing—review and editing, I.K.; supervision, S.T.M.-D. All the authors contributed to the manuscript equally.

Funding: This research received no external funding.

Acknowledgments: The second and third authors thank the Deanship of Scientific Research and Deanship of Community Service at Majmaah University, Kingdom of Saudi Arabia for supporting this work. The authors are also thankful to students (Jilan Hatem Al Harbi; Raheq Saud al-Makhmali; Raghad Mohamed Al-Tawala; Janna Hamad Al-Misnad; Ritaj Al Mutairi) for participating in this work.

Conflicts of Interest: The authors declare no conflict of interest.

Nomenclature

$U(x)$	Main stream velocity	u	u component of the velocity
v	v component of the velocity	μ_{nf}	Effective dynamic viscosity
ρ_{nf}	Effective density	k_{nf}	Effective thermal conductivity
$(\rho c_p)_{nf}$	Effective heat capacity	k_s	Thermal conductivity of nanoparticles
k_f	Thermal conductivity of the base fluid	ρ_s	Density of the nanoparticles
ρ_f	Density of the base fluid	ϕ	Volume fraction of the nanoparticles
T	Temperature	λ	Hartree pressure gradient parameter
η	Similarity variable	$F(\eta)$	Dimensionless velocity
$\beta(\eta)$	Dimensionless temperature	Pr	Prandtl number
Ec	Eckert number	Rd	Thermal radiation parameter

References

1. Rajagopal, K.R.; Gupta, A.S.; Na, T.Y. A note on the Falkner-Skan flows of a non-Newtonian fluid. *Int. J. Non-Linear Mech.* **1983**, *18*, 313–320. [[CrossRef](#)]
2. Falkner, V.M.; Skan, S.W. Some approximate solutions of the boundary layer equations. *Philos. Mag.* **1931**, *12*, 865–896. [[CrossRef](#)]
3. Falkner, V.M.; Skan, S.W. Some approximate solutions of the boundary-layer for flow past a stretching boundary. *SIAM J. Appl. Math.* **1931**, *49*, 1350–1358.
4. Hartree, D.H. On an equation occurring in Falkner and Skan's approximate treatment of the equations of the boundary layer. *Proc. Camb. Philos. Soc.* **1937**, *33*, 223–239. [[CrossRef](#)]
5. Lin, H.T.; Lin, L.K. Similarity solutions for laminar forced convection heat transfer from wedges to fluids of any Prandtl number. *Int. J. Heat Mass Transf.* **1987**, *30*, 1111–1118. [[CrossRef](#)]
6. Watanabe, T. Thermal boundary layer over wedge with uniform suction or injection in force flow. *Acta Mech.* **1990**, *83*, 119–126. [[CrossRef](#)]
7. Watanabe, T.; Pop, I. Magnetohydrodynamic free convection flow over a wedge in the presence of a transverse magnetic field. *Int. Commun. Heat Mass Transf.* **1993**, *20*, 871–881. [[CrossRef](#)]
8. Koh, J.C.Y.; Hartnett, J.P. Skin-friction and heat transfer for incompressible laminar flow over porous wedges with suction and variable wall temperature. *Int. J. Heat Mass Transf.* **1961**, *2*, 185–198. [[CrossRef](#)]
9. Kumari, M.; Takhar, H.S.; Nath, G. Mixed convection flow over a vertical wedge embedded in a highly porous medium. *Heat Mass Transf.* **2001**, *37*, 139–146. [[CrossRef](#)]
10. Chamkha, A.J.; Mujtaba, M.; Quadri, A.; Issa, C. Thermal radiation effects on MHD forced convection flow adjacent to a non-isothermal wedge in the presence of a heat source or sink. *Heat Mass Transf.* **2003**, *39*, 305–312. [[CrossRef](#)]
11. El-dabe, N.T.; Ghaly, A.Y.; Rizkallah, R.R.; Eweis, K.M. Numerical solution of MHD boundary layer flow of non-newtonian Casson fluid on a moving wedge with heat and mass transfer and induced magnetic field. *J. Appl. Math. Phys.* **2015**, *3*, 649–663. [[CrossRef](#)]
12. Ishak, A.; Nazar, R.; Pop, I. Falkner-Skan equation for flow past a moving wedge with suction or injection. *J. Appl. Math. Comput.* **2007**, *25*, 67–83. [[CrossRef](#)]
13. Ishak, A.; Nazar, R.; Pop, I. Moving wedge and flat plate in a micropolar fluid. *Int. J. Eng. Sci.* **2006**, *44*, 1225–1236. [[CrossRef](#)]

14. Rashidi, M.M.; Ali, M.; Freidoonimehr, N.; Rostami, B.; Hossain, M.A. Mixed Convective Heat Transfer for MHD Viscoelastic Fluid Flow over a Porous Wedge with Thermal Radiation. *Adv. Mech. Eng.* **2014**, *6*, 735939. [[CrossRef](#)]
15. Su, X.; Zheng, L.; Zhang, X.; Zhang, J. MHD mixed convective heat transfer over a permeable stretching wedge with thermal radiation and ohmic heating. *Chem. Eng. Sci.* **2012**, *78*, 1–8. [[CrossRef](#)]
16. Mukhopadhyay, S.; Mondal, I.C.; Chamkha, A.J. Casson fluid flow and heat transfer past a symmetric wedge. *Heat Transf. Res.* **2013**, *42*, 665–675. [[CrossRef](#)]
17. Hussanan, A.; Ismail, Z.; Khan, I.; Hussein, A.G.; Shafie, S. Unsteady boundary layer MHD free convection flow in a porous medium with constant mass diffusion and Newtonian heating. *Eur. Phys. J. Plus* **2014**, *129*, 46. [[CrossRef](#)]
18. Kandasamy, R.; Raji, A.W.B.M.; Khamis, A.B. Effects of chemical reaction, heat and mass transfer on boundary layer flow over a porous wedge with heat radiation in the presence of suction or injection. *Theor. Appl. Mech.* **2006**, *33*, 123–148. [[CrossRef](#)]
19. Chambre, P.L.; Acrivos, A. Diffusion of a chemically reactive species in a laminar boundary layer flow. *Indian Eng. Chem.* **1957**, *49*, 1025. [[CrossRef](#)]
20. Hussanan, A.; Anwar, M.I.; Ali, F.; Khan, I.; Shafie, S. Natural convection flow past an oscillating plate with Newtonian heating. *Heat Transf. Res.* **2014**, *45*, 119–135. [[CrossRef](#)]
21. Su, X.; Zheng, L. Hall effect on MHD flow and heat transfer of nanofluids over a stretching wedge in the presence of velocity slip and Joule heating. *Cent. Eur. J. Phys.* **2013**, *11*, 1694–1703. [[CrossRef](#)]
22. Pal, D.; Mondal, H. Influence of temperature-dependent viscosity and thermal radiation on MHD forced convection over a non-isothermal wedge. *Appl. Math. Comput.* **2009**, *212*, 194–208. [[CrossRef](#)]
23. Rahman, M.M.; Al-Lawatia, M.A.; Eltayeb, I.A.; Al-Salti, N. Hydromagnetic slip flow of water based nanofluids past a wedge with convective surface in the presence of heat generation (or) absorption. *Int. J. Therm. Sci.* **2012**, *57*, 172–182. [[CrossRef](#)]
24. Yacob, N.A.; Ishak, A.; Pop, I. Falkner-Skan problem for a static or moving wedge in nanoliquids. *Int. J. Therm. Sci.* **2011**, *50*, 133–139. [[CrossRef](#)]
25. Khan, U.; Ahmed, N.; Mohyud-Din, S.T. Influence of viscous dissipation and Joule heating on MHD bio-convection flow over a porous wedge in the presence of nanoparticles and gyrotactic microorganisms. *SpringerPlus* **2016**, *5*, 2043. [[CrossRef](#)] [[PubMed](#)]
26. Ahmed, N.; Khan, U.; Mohyud-Din, S.T. Heat transfer enhancement in hydromagnetic dissipative flow past a moving wedge suspended by H₂O-aluminum alloy nanoparticles in the presence of thermal radiation. *Int. J. Hydrogen Energy* **2017**, *42*, 24634–24644. [[CrossRef](#)]
27. Ullah, I.; Bhattacharyya, K.; Shafie, S.; Khan, I. Unsteady MHD Mixed Convection Slip Flow of Casson Fluid over Nonlinearly Stretching Sheet Embedded in a Porous Medium with Chemical Reaction, Thermal Radiation, Heat Generation/Absorption and Convective Boundary Conditions. *PLoS ONE* **2016**, *10*, e0165348. [[CrossRef](#)]
28. Khalid, A.; Khan, I.; Shafie, S. Heat transfer in ferrofluid with cylindrical shape nanoparticles past a vertical plate with ramped wall temperature embedded in a porous medium. *J. Mol. Liq.* **2016**, *221*, 1175–1183. [[CrossRef](#)]
29. Aman, S.; Khan, I.; Ismail, Z.; Salleh, M.Z. Impacts of gold nanoparticles on MHD mixed convection Poiseuille flow of nanofluid passing through a porous medium in the presence of thermal radiation, thermal diffusion and chemical reaction. *Neural Comput. Appl.* **2016**, *30*, 789–797. [[CrossRef](#)]
30. Ahmed, N.; Khan, U.; Mohyud-Din, S.T. Thermo-diffusion and Diffusion-Thermo effects on Flow of Second Grade fluid between two Inclined plane Walls. *J. Mol. Liq.* **2016**, *224*, 1074–1082.
31. Ahmed, N.; Khan, U.; Mohyud-Din, S.T. Influence of Thermal Radiation and Viscous dissipation on Squeezed flow of Water between Riga Plates saturated with Carbon nanotubes. *Colloids Surf. A Physicochem. Eng. Asp.* **2017**, *522*, 389–398. [[CrossRef](#)]
32. Ahmed, N.; Khan, U.; Mohyud-Din, S.T. Influence of an Effective Prandtl number Model on Squeezed Flow of $\gamma\text{Al}_2\text{O}_3\text{-H}_2\text{O}$ and $\gamma\text{Al}_2\text{O}_3\text{-C}_2\text{H}_6\text{O}_2$ Nanofluids. *J. Mol. Liq.* **2017**, *238*, 447–454. [[CrossRef](#)]
33. Asadullah, M.; Khan, U.; Ahmed, N.; Mohyud-Din, S.T. Analytical and Numerical Investigation of Thermal Radiation effects on Flow of viscous Incompressible fluid with Stretchable Convergent/divergent Channels. *J. Mol. Liq.* **2016**, *224*, 768–775.

34. Gul, A.; Khan, I.; Shafie, S.; Khalid, A.; Khan, A. Heat Transfer in MHD Mixed Convection Flow of a Ferrofluid Along a Vertical Channel. *PLoS ONE* **2015**, *11*, e0141213. [[CrossRef](#)]
35. Zin, M.; Athirah, N.; Khan, I.; Shafie, S. The impact silver nanoparticles on MHD free convection flow of Jeffery fluid over an oscillating vertical plate embedded in a porous medium. *J. Mol. Liq.* **2016**, *222*, 138–150.
36. Gul, A.; Khan, I.; Shafie, S. Energy Transfer in Mixed Convection MHD Flow of Nanofluid Containing Different Shapes of Nanoparticles in a Channel Filled with Saturated Porous Medium. *Nanoscale Res. Lett.* **2015**, *10*, 490.
37. Ali, F.; Gohar, M.; Khan, I. MHD flow of water-based Brinkman type nanofluid over a vertical plate embedded in a porous medium with variable surface velocity, temperature and concentration. *J. Mol. Liq.* **2016**, *223*, 412–419. [[CrossRef](#)]
38. Ullah, I.; Shafie, S.; Khan, I. Effects of slip condition and Newtonian heating on MHD flow of Casson fluid over a nonlinearly stretching sheet saturated in a porous medium. *J. King Saud Univ.* **2016**, *29*, 250–259. [[CrossRef](#)]
39. Ullah, I.; Khan, I.; Shafie, S. MHD Natural Convection Flow of Casson Nanofluid over Nonlinearly Stretching Sheet Through Porous Medium with Chemical Reaction and Thermal Radiation. *Nanoscale Res. Lett.* **2016**, *11*, 527. [[CrossRef](#)]
40. Sheikholeslami, M.; Shehzad, S.A. Magnetohydrodynamic nanofluid convection in a porous enclosure considering heat flux boundary condition. *Int. J. Heat Mass Transf.* **2017**, *106*, 1261–1269. [[CrossRef](#)]
41. Sheikholeslami, M.; Hayat, T.; Alsaedi, A. Numerical study for external magnetic source influence on water based nanofluid convective heat transfer. *Int. J. Heat Mass Transf.* **2017**, *106*, 745–755. [[CrossRef](#)]
42. Sheikholeslami, M.; Vajravelu, K. Nanofluid flow and heat transfer in a cavity with variable magnetic field. *Appl. Math. Comput.* **2017**, *298*, 272–282. [[CrossRef](#)]
43. Ahmed, N.; Khan, U.; Mohyud-Din, S.T.; Waheed, A. Shape effects of nanoparticles on Squeezed flow between two Riga Plates in the presence of thermal radiation. *Eur. Phys. J. Plus* **2017**, *132*, 321. [[CrossRef](#)]
44. Ahmed, N.; Khan, U.; Mohyud-Din, S.T.; Manzoor, R. Influence of Viscous dissipation on Copper Oxide Nanofluid in an Oblique Channel: Implementation of KKL Model. *Eur. Phys. J. Plus* **2017**, *132*, 237. [[CrossRef](#)]
45. Bin-Mohsin, B.; Ahmed, N.; Khan, U.; Mohyud-Din, S.T. A Bioconvection Model for squeezing flow of nanofluid Between parallel plates in the presence gyrotactic microorganisms. *Eur. Phys. J. Plus* **2017**, *132*, 187. [[CrossRef](#)]
46. Ullah, I.; Khan, I.; Shafie, S. Hydromagnetic Falkner-Skan flow of Casson fluid past a moving wedge with heat transfer. *Alex. Eng. J.* **2016**, *55*, 2139–2148. [[CrossRef](#)]
47. Srinivasacharya, D.; Mendu, U.; Venumadhav, K. MHD Boundary Layer Flow of a Nanofluid Past a Wedge. *Procedia Eng.* **2015**, *127*, 1064–1070. [[CrossRef](#)]
48. Sandeep, N.; Sharma, R.P.; Ferdows, M. Enhanced heat transfer in unsteady magnetohydrodynamic Enhanced heat transfer in unsteady magnetohydrodynamic. *J. Mol. Liq.* **2017**, *234*, 437–443. [[CrossRef](#)]
49. Haq, R.U.; Noor, N.F.M.; Khan, Z.H. Numerical simulation of water based magnetite nanoparticles between two parallel disks. *Adv. Powder Technol.* **2016**, *27*, 1568–1575. [[CrossRef](#)]
50. Rashidi, M.M.; Ganesh, V.N.; Abdul, H.A.K.; Ganga, B.; Lorenzini, G. Influences of an effective Prandtl number model on nano boundary layer flow of $gAl_2O_3-H_2O$ and $gAl_2O_3-C_2H_6O_2$ over a vertical stretching sheet. *Int. J. Heat Mass Transf.* **2016**, *98*, 616–623. [[CrossRef](#)]
51. Khan, U.; Ahmed, N.; Mohy-ud-Din, S.T. Numerical investigation for three dimensional squeezing flow of nanofluid in a rotating channel with lower stretching wall suspended by carbon nanotubes. *Appl. Therm. Eng.* **2017**, *113*, 1107–1117. [[CrossRef](#)]
52. Ganapathirao, M.; Ravindran, R.; Momoniat, E. Effects of chemical reaction, heat and mass transfer on an unsteady mixed convection boundary layer flow over a wedge with heat generation/absorption in the presence of suction or injection. *Int. J. Heat Mass Transf.* **2015**, *51*, 289–300. [[CrossRef](#)]

